[AMERICAN JOURNAL OF SCIENCE, VOL. 266, OCTOBER 1968, P. 704-727]

THE OXYGEN FUGACITY OF ALKALINE BASALT AND RELATED MAGMAS, TRISTAN DA CUNHA*

A. T. ANDERSON

U. S. Geological Survey, Washington, D. C. 20242

ABSTRACT. Compositions of intergrown, phenocrystic titaniferous magnetite and ferrian ilmenite determined by electron probe X-ray microanalysis within 10 microns of their interface permit application of the data of Lindsley to delimit the temperatures and oxygen fugacities of alkaline magmas of Tristan da Cunha as follow:

trachybasalt (specimen 622): $\log_{10} f_{O_2} \leqslant 9.0 - \frac{24900}{T°K}$

trachybasalt (specimen 347): $\log_{10} f_{O_2} \leqslant 15.8 - \frac{34400}{T°K}$

trachyandesite (specimen 486): $1110°C$, $f_{O_2} \leqslant 10^{-7.8}$

trachyte (specimen 560): $930°C$, $f_{O_2} \leqslant 10^{-11.7}$.

Neither specimen of trachybasalt (specimens 622 and 347) contains discrete phenocrystic ferrian ilmenite. The ferrian ilmenite is contained within titaniferous magnetite or augite. The composition of the ferrian ilmenite in trachybasalt (basalt 622) ranges between Hm 27 (mole percent Fe_2O_3) in its interior and Hm 15 at its contact with titaniferous magnetite. Similarly, the composition of the titaniferous magnetite in trachybasalt (specimen 622) ranges between Usp 19 (mole percent Fe_2TiO_4) in its interior and Usp 65 near its contact with ferrian ilmenite. These textures and compositional ranges indicate that the ferrian ilmenite in trachybasalt was reduced by the liquid and not produced by oxidation of the conterminous titaniferous magnetite. The Mg contents and Hm values of the ferrian ilmenite in trachybasalt overlap those of the ferrian ilmenite phenocrysts in trachyandesite and trachyte. Thus the ferrian ilmenite in trachybasalt may be derived from fractionated and oxidized residual magma or rock. Consequently the deduced oxygen fugacities are maxima for the trachybasalt liquids.

The oxygen fugacity—temperature relationship found for trachybasalt, which contains ferrian ilmenite, is within a factor of 3 of that of Hawaiian subalkaline (tholeiitic) basalt. This close similarity is unexpected in view of the substantial differences in their Fe_2O_3/FeO ratios but can be qualitatively explained in terms of differences in melt basicity. The similarity implies similar f_{O_2}—T environments of origin of alkaline and subalkaline basaltic liquids.

INTRODUCTION

Terminology. The words that describe the iron-titanium oxide minerals are defined as follows (following Buddington, Fahey, and Vlisidis, 1963):

titaniferous magnetite: an optically homogeneous Fe-Ti spinel phase having an oxide stoichiometry approximately R_3O_4.

ilmeno-magnetite: a regular intergrowth of titaniferous magnetite and ferrian-ilmenite, titan-hematite, or meta-ilmenite.

ferrian-ilmenite: an optically homogeneous Fe-Ti rhombohedral phase having an oxide stoichiometry essentially R_2O_3 with Hm (mole percent Fe_2O_3) less than 50 percent.

titan-hematite: same as ferrian-ilmenite but with Hm greater than 50 percent.

meta-ilmenite: an optically mottled, submicroscopic intergrowth of presumed titan-hematite and rutile.

* Publication authorized by the Director, U. S. Geological Survey.

pseudobrookite: an optically homogeneous Fe-Ti orthorhombic phase with an oxide stroichiometry near R_3O_5 and mole percent of Fe_2TiO_5 greater than 50.

ferro-pseudobrookite: same as pseudobrookite but mole percent of Fe_2TiO_5 less than 50.

The word *phenocryst* is here used in a narrower sense than is customary to describe a crystal that is easily visible with the naked eye in an otherwise aphanitic rock. A wholly aphanitic rock may contain microphenocrysts, and a wholly phaneritic rock may contain megacrysts, porphyrocrysts, or insets. Phenocrysts, so defined, are presumed to have crystallized previous to eruption and before final quenching of the magma near the surface. Very great size contrast between phenocryst (generally larger than 0.2 mm in diameter) and groundmass crystals (mostly less than 0.01 mm) and occurrence in glassy lava are the bases for this presumption.

Alkaline and *subalkaline* basalt are used in the sense defined by Chayes (1966). Specific names of rocks from Tristan da Cunha (trachybasalt, trachyandesite, and trachyte) are taken from Baker and others (1964) and are based on alkali and silica contents as defined by Le Maitre (1962).

General statement. Knowledge of the oxygen fugacity of basalt magmas can provide a fuller understanding of their mode of origin. The following four factors can be expected to influence the oxygen fugacity of a basalt magma:

1. the compositions of phases present and the extent of fractional melting at the site of magma generation,
2. the change in temperature and pressure due to ascent of the magma from the site of generation to that of eruption,
3. losses from and additions to the magma during ascent,
4. crystallization in the magma prior to eruption.

The purpose of this paper is to establish the oxygen fugacity of an oceanic alkaline basalt in order that it may be compared with that of other types of basalt and with the results of experiment in the context of the factors listed above.

The oxygen fugacity and temperature of a magma can be deduced from the analysis of co-equilibrated iron-titanium oxide minerals (Buddington and Lindsley, 1964). Analysis of iron-titanium oxide phenocrysts, which crystallized intratellurically, advantageously minimizes the effects, during and subsequent to eruption, of contamination of the magma by air or water and of loss of juvenile gas.

Any reaction between phenocrysts and *liquid* which may occur subsequent to eruption but prior to solidification is assumed to take place without communication with outside oxidation and reduction agents. This assumption is consistent with the subsolidus temperature range over which oxidation apparently occurs in Hawaiian and Icelandic basalt (Sato and Wright, 1966; Watkins and Haggerty, 1967).

It is hereby reemphasized that this study is concerned with phenocrysts of titaniferous magnetite and ferrian ilmenite that were selected because they lack visible products of oxidation. In some of the rocks studied some of the phenocrysts of titaniferous magnetite are partly converted to ilmeno-magnetite, particularly where the phenocryst borders on a vesicular cavity or major crack. Phenocrysts of titaniferous magnetite that are partly oxidized to ilmeno-magnetite were not analyzed in this investigation.

Geologic setting. The rocks studied are from Tristan da Cunha island (hereafter abbreviated to Tristan) in the central south Atlantic ocean and are members of the oceanic alkaline basalt-trachyte series. The geology and petrology of Tristan were subjects of a recent monograph by Baker and others (1964). Lavas dominate the sea cliffs and the lower slopes of Tristan, but the steep slopes above about 2500 feet elevation are primarily composed of pyroclastic rocks. The principle rock types on the island are trachybasalt and trachyandesite. There are lesser amounts of ankaramite, alkali basalt, and trachyte. The chemical relationships between trachybasalt, trachyandesite, and trachyte suggest them to be related to chemically similar parent magmas by means of crystallization differentiation (Baker and others, 1964). The more fractionated rocks, trachyandesite and trachyte, are principally in parasitic pyroclastic centers interbedded with the basalts (Baker and others, 1964; Gass, 1967). The lavas are commonly porphyritic. The principal phenocrysts are plagioclase, augite, and titaniferous magnetite. Phenocrystic olivine, sphene, and apatite are rare, and amphibole is generally subordinate to augite. Coarse-grained xenoliths found in the lavas and dike rocks of Tristan are composed of variable proportions of plagioclase, augite, amphibole, biotite, and ilmeno-magnetite (Baker and others, 1964).

Analytical conditions and calculation procedures. The analyses were made with electron probe X-ray microanalyzers. The operating conditions, correction factors, and standards used and their analyses are listed in tables 1 to 3. The correction procedures are almost identical to those used by Carmichael (1967) and are due to Smith (1965). The accuracy of the analyses is estimated to be $\pm$ 2 percent of the amount present for Fe and Ti and $\pm$ 5 percent of the amount present for Mg, Al, and Mn.

TABLE 1

Microprobe standards, operating conditions, and correction factors used for ilmenite analyses

Element	Standard	Operating conditions		Correction factors	
		Voltage	Specimen current	Absorption	Atomic No.
Mg	K13-131.8 il	15 KV	0.05×10^{-6} amp	1.00	1.00
Fe	K13-131.8 il	15 KV	0.05×10^{-6} amp	1.00	1.00
Ti	K13-131.8 il	15 KV	0.05×10^{-6} amp	1.00	1.00
Mn	Mn_2SiO_4	20 KV	0.2×10^{-6} amp	1.02	0.99
Al	61-1436 cr	15 KV	0.05×10^{-6} amp	1.19	1.00

TABLE 2

Microprobe standards, operating conditions, and correction factors used for magnetite analyses

Element	Standard	Operating conditions		Correction factors		
		Voltage	Specimen current	Absorption	Atomic No.	Dead time
Mg	K13-131.8 il	15 kv	0.05 × 10^{-6} amp	1.07	1.00	
Al	61-1436 cr	15 kv	0.05 × 10^{-6} amp	1.19	1.00	
Fe*	L4-175 mt	15 kv	0.05 × 10^{-6} amp	1.00	1.00	
Fe*	K12-131.8 il	15 kv	0.02-0.05 × 10^{-6} amp	0.98	0.97	1.02
Ti*	L4-175 mt	15 kv	0.05 × 10^{-6} amp	1.00	1.00	
Ti*	K13-131.8 il	15 kv	0.02-0.05 × 10^{-6} amp	1.005	0.98	0.97
Mn	Mn_2SiO_4	20 kv	0.2 × 10^{-6} amp	1.01	0.99	
V	V metal	20 kv	0.2 × 10^{-6} amp	1.00	1.06	

* Fe and Ti analyses of specimens 117a, 125, 572, 560, 486, 491, and 68 are relative to the magnetite standard. All other Fe and Ti analyses of magnetites are reported relative to the ilmenite standard. Analysis of the magnetite standard, L4-175, relative to the ilmenite, K13-131.8, yields 54.9 percent Fe and 12.2 percent Ti, each within 1 percent of that reported by Z. Katzendorfer and H. Boileau (Quebec Dept. Nat. Resources).

TABLE 3

Analyses of reference standards used for microprobe analyses of magnetite and ilmenite

	L4-175* Magnetite	K13-131.8* Ilmenite	61-1436** Chromite	Tephroite***
Ti	12.3	31.4	0.35	
Fe^{+3}	19.6	2.85	6.1	
Fe^{+2}	34.8	29.8	15.1	2.6
Al	1.67	0.0	9.7	
Mg	1.59	2.42	6.02	0.3
Cr	0.13	0.02	28.3	
V	0.18	0.02	0.21	
Mn	0.30	0.43	0.62	(48.3)
Ni	0.05	0.01	0.12	
Ca	0.08	0.04	0.06	
Si	0.03	0.08	0.12	
Oxide Sum	100.10	100.32	100.29	100.0

* Natural magnetite-ulvospinel and ilmenite from titaniferous magnetite deposits in labradorite anorthosite, Quebec. Small quantities are available from the author upon request. Z. Katzendorfer and H. Boileau (Quebec Department of Natural Resources), analysts. The ilmenite analysis by Katzendorfer and Boileau showed 0.7 wt percent Al and 31.0 percent Ti. Microprobe results indicate an Al content less than 0.1 percent and 31.4 percent Ti relative to the writer's A128 ilmenite standard (Anderson, in press). These latter values have been assumed in this work.

** Natural chromite, slightly variable in composition, collected by E. N. Cameron, supplied by J. V. Smith, C. O. Ingamells (Pennsylvania State University), analyst.

*** Natural tephroite collected by Brian Mason, supplied by J. V. Smith. Fe and Mg by microprobe analysis, Mn by difference, analysis by the author.

Oxide formula totals provide a summation test of the analytical accuracy and define the mole fractions of Fe_2TiO_4 (Usp) in titaniferous magnetite and of Fe_2O_3 (Hm) in ferrian ilmenite. Stoichiometry is assumed for both spinel (R_3O_4) and rhombohedral oxide (R_2O_3). The effect of the stoichiometry assumption on the deduced Hm and Usp values can be seen on figure 1. Points A′, B′, and C′ are the calculated compositions corresponding to postulated real compositions at A, B, and C. Additional assumptions are required to deduce the mole fractions of Usp and Hm that most closely correspond to those of coexisting titaniferous magnetite and ferrian ilmenite in the system $FeO + Fe_2O_3 + TiO_2$ (Buddington and Lindsley, 1964, p. 327-329). For spinels these assumptions are:

1. Al is allotted to $Mg_{0.7}Fe_{0.3}Al_2O_4$.
2. remaining Mg is allotted to Mg_2TiO_4.
3. Mn is calculated as Mn_2TiO_4.
4. Usp = mole percent Fe_2TiO_4/(mole percent Fe_2TiO_4 + mole percent Fe_3O_4).

For ferrian ilmenites the additional assumptions are:

1. Mg and Mn are calculated as $MgTiO_3$ and $MnTiO_3$.
2. Hm = mole percent Fe_2O_3/(mole percent Fe_2O_3 + mole percent $FeTiO_2$).

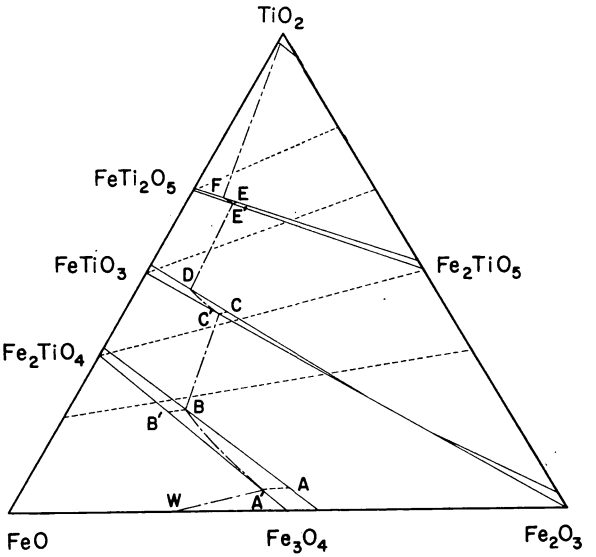

Fig. 1. Diagrammatic phase diagram of the system: TiO_2 + FeO + Fe_2O_3 at about 1200°C (from Webster and Bright, 1961; Taylor, 1964). The line W-A'-B-C'-D-E'-F-TiO_2 is an oxygen fugacity isobar. Lines A-A', B-B', and C-C' join points representing real (A, B, and C) and calculated (A', B', and C') compositions as discussed in the text (p. 708). The short dash lines are lines of equal Fe/Ti ratio.

The bases for these assumptions are the experiments of Speidel (1967 and written commun.) and analyses of coarsely exsolved magnetite + ulvospinel + spinel intergrowths (Anderson, in press). These assumptions give good agreement between the temperature and oxygen fugacity deduced for a natural lava lake from Hawaii by analysis of magnetite and ilmenite (Wright and Weiblen, 1967) and from direct thermocouple and electrochemical measurement (Sato and Wright, 1966).

An important uncertainty in the present work is the analytical resolution of the magnetite and ilmenite near their contact with each other. The resolution is probably poorest for titanium $K\alpha$ radiation which is not much absorbed and for which the operating voltage is considerably greater than the critical excitation voltage. It is possible that the reported Ti contents of analyzed magnetite near ilmenite are high and that the Ti content of ilmenite near magnetite is low. It is difficult to assess the magnitude of these uncertainties, but the *increase* in Ti content of ferrian ilmenite as magnetite is approached (fig. 2; table 6) suggests that the effect is not significant more than 5 microns from the interface.

RESULTS

Titaniferous magnetite is the only iron-titanium oxide phenocryst in the trachybasalts. In specimens 117a and 125 the observed compositions are Usp 44 to 45 and Usp 54 to 57, respectively (table 4).

Two exceptional trachybasalts (specimens 622 and 347) contain rare, complex phenocrysts which consist of strongly zoned titaniferous magne-

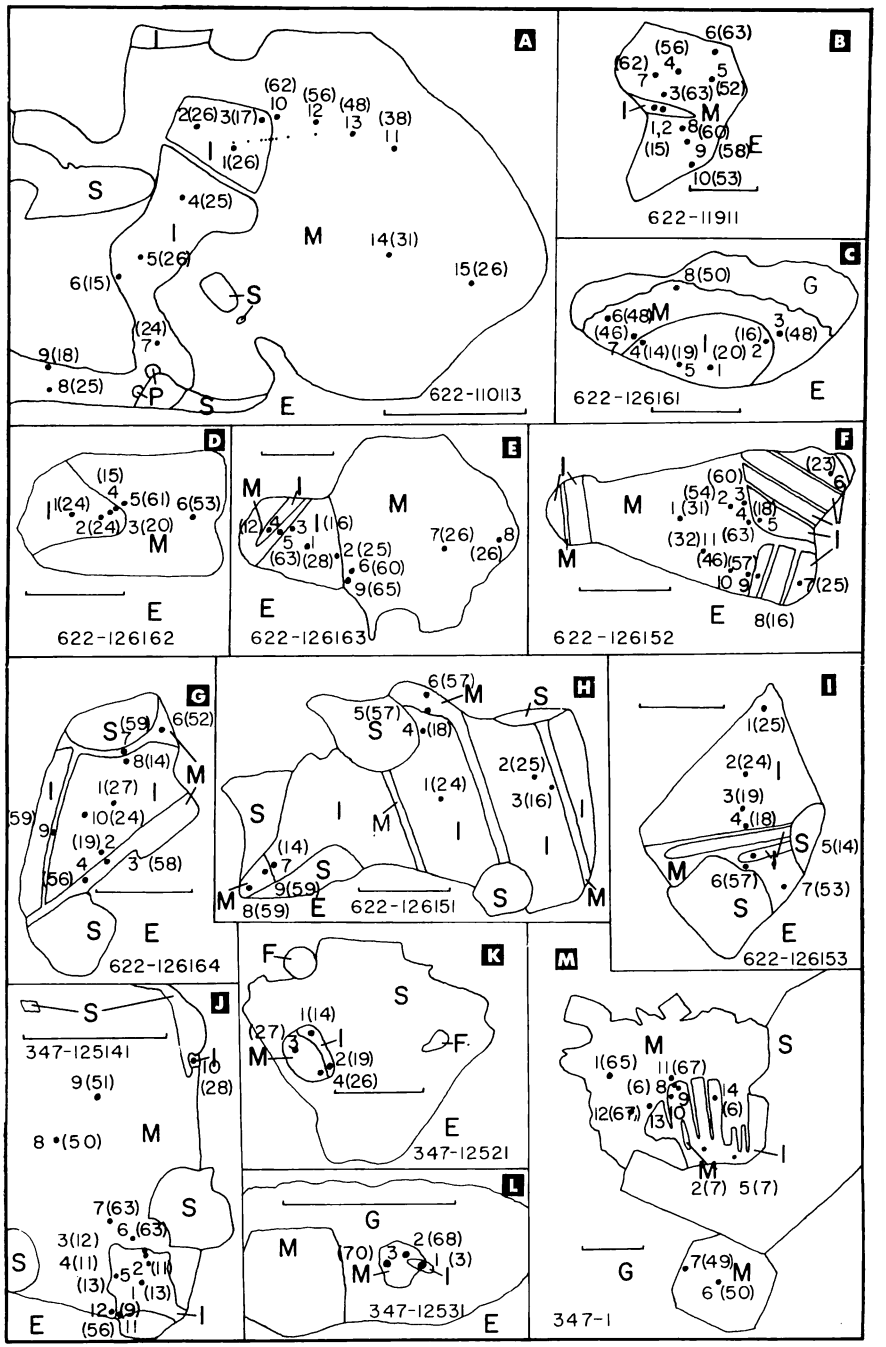

Fig. 2. Diagrams showing phenocrysts of intergrown titaniferous magnetite and ilmenite in trachybasalts (from specimens 622 and 347). Numbered circles correspond to analyses in tables 5, 6, and 7. Figures in parentheses are Usp and Hm values determined at the particular sites. E, epoxy plastic mounting medium; F, ?iron hydroxide; G, groundmass; I, ferrian ilmenite; M, titaniferous magnetite; P, pyrrhotite; S, silicate (mostly augite). The bar in each inset is 100 microns long.

TABLE 4

Analyses of titaniferous magnetite in trachybasalts 117a and 125

Designation*	Mg**	Mn**	Al**	Ti**	Fe **	R_2O_3*** sum	Usp‡	Remarks
117a-1-1	2.4	0.8	1.3	10.1	54.3	98.4	45	phenocryst interior
117a-1-2	2.5	0.9	1.9	10.4	53.9	98.9	45	phenocryst interior
117a-1-3	2.6	0.8	1.8	10.5	54.2	99.3	45	phenocryst margin
117a-1-4	2.7	0.8	1.7	10.5	54.7	100.0	44	phenocryst margin
125-1-1	2.5	0.8	1.7	11.9	51.2	96.5	54	phenocryst interior
125-1-2	2.6	0.8	1.8	12.7	52.2	99.5	57	phenocryst intermediate
125-1-3	2.6	0.7	1.6	12.7	51.9	98.9	57	phenocryst margin
125-1-4	2.6	0.8	1.6	12.8	52.8	100.5	56	phenocryst margin
125-2	1.4	1.1	0.5	13.3	54.1	99.1	60	groundmass crystal
125-3-1	2.6	0.9	1.9	12.6	55.2	104.2	54	phenocryst margin
125-3-2	2.9	0.8	1.6	12.7	53.9	102.3	54	phenocryst interior

* The two numbers following the specimen number refer to grain number and spot number.

** The values given are weight percents of the elements corrected as explained in the text (p. 706-708) and on tables 1 and 2.

*** The R_3O_4 sum is the weight sum of the oxide formulae as explained in the text (p. 706-708).

‡ The mole percent of Fe_2TiO_4 (Usp) is calculated as explained in the text (p. 706-708).

tite irregularly intergrown with zoned ferrian ilmenite (tables 5, 6, and 7). These two specimens are the most significant ones as far as this investigation is concerned, because they are the only basalts that contain coexisting titaniferous magnetite and ferrian ilmenite, thus permitting their oxygen fugacity and temperature to be determined. A detailed description follows of the iron-titanium oxide phenocrysts in these two specimens:

Phenocrysts of titaniferous magnetite, which lack intergrown ilmenite, predominate in both trachybasalts (specimens 622 and 347). Of about 300 phenocrysts examined from each rock, trachybasalt specimen 622 contained about 20 with intergrown ilmenite, trachybasalt specimen 347 had only 3 such phenocrysts. In these specimens nearly all titaniferous magnetite phenocrysts are strongly zoned. The maximum range in composition is Usp 19 to Usp 65 in trachybasalt specimen 622 and Usp 26 to Usp 67 in trachybasalt specimen 347 (table 5 and fig. 2). Low values of Usp are in the interiors of a few phenocrysts and at maximum distance away from intergrown ilmenite. The high Usp values are near intergrown ilmenite, near the outer margins of large crystals, and in small crystals (microphenocrysts). In both rocks the highest Usp values occur in groundmass magnetites. The intergrown ferrian ilmenite decreases in Hm content from about Hm 27 to Hm 15 as the contact with titaniferous magnetite is approached (for example, fig. 2A; tables 6 and 7).

Tables 8 and 9 list the analyses of the coexisting titaniferous magnetite and ferrian ilmenite phenocrysts in trachyandesite specimens 572, 486, 491, and 68 and in trachyte specimen 560.

TABLE 5

Analyses of titaniferous magnetite in trachybasalts 622 and 347

Designation*	Mg**	Mn**	Al**	Ti**	Fe **	R_2O_3*** sum	Usp‡	Remarks
622-110113-10	2.4		1.2	13.1	52.1	97.6	62	see figure 2A
622-110113-11	2.1		2.3	8.5	56.8	99.6	38	see figure 2A
622-110113-12	2.3	0.56	1.4	12.1	53.0	97.5	56	see figure 2A
622-110113-13	2.5		1.5	10.9	54.7	98.8	48	see figure 2A
622-110113-14	1.6	0.46	2.3	6.8	59.3	99.3	31	see figure 2A
622-110113-15	1.6	0.46	2.0	6.1	60.6	100.1	26	see figure 2A
622-11911-3	3.9		2.1	14.1	48.6	98.6	63	see figure 2B
622-11911-4	3.8		3.1	12.4	50.0	99.8	56	see figure 2B
622-11911-5	3.6		3.3	11.4	51.0	99.4	52	see figure 2B
622-11911-6	3.1		3.4	11.4	52.0	100.2	53	see figure 2B
622-11911-7	3.6		2.4	13.7	49.6	99.3	62	see figure 2B
622-11911-8	3.7		2.4	13.4	49.6	99.1	60	see figure 2B
622-11911-9	3.7		2.4	13.2	49.7	98.9	59	see figure 2B
622-11911-10	3.7		2.7	12.1	50.9	99.5	53	see figure 2B
622-110111-1	3.6		4.0	8.5	52.8	99.1	37	phenocryst interior
622-110111-2	3.8		4.0	8.6	52.9	99.8	37	phenocryst interior
622-110111-3	2.9		3.3	10.9	51.5	98.0	52	phenocryst margin
622-110112-1	3.7		4.4	8.6	52.5	99.8	38	phenocryst intermediate
622-110112-2	3.7		4.5	8.4	52.4	99.3	36	phenocryst interior
622-110112-3	2.7		3.3	11.1	51.9	98.6	54	phenocryst margin
622-110114-1	1.4	0.58	2.0	6.4	61.3	99.8	28	phenocryst interior
622-110114-2	1.3		2.0	6.2	61.7	100.1	29	phenocryst interior
622-110114-3	1.9		2.5	6.9	59.0	99.5	31	phenocryst intermediate
622-110114-4	2.6		3.3	10.0	53.3	98.9	48	phenocryst margin
622-110114-5	2.3		2.9	8.4	56.9	100.1	38	phenocryst intermediate
622-110115-1	3.6	0.54	4.0	10.5	50.8	99.8	48	phenocryst interior
622-110115-2	3.4		3.6	11.4	51.2	99.9	53	phenocryst intermediate
622-110115-3	2.8		3.1	12.0	50.8	97.9	58	phenocryst margin
622-11912-1	3.7		3.7	9.0	53.4	100.2	38	phenocryst interior
622-11912-2	3.2		3.7	11.1	52.3	100.8	52	phenocryst margin
622-11912-3	3.6		4.0	9.0	53.4	100.4	39	phenocryst intermediate
622-11912-4	3.6		3.8	8.8	53.2	99.7	38	phenocryst adjacent to pyrrhotite
622-11912-5	4.1			8.8	54.0	94.7	28	phenocryst 15μ from pyrrhotite
622-11913-1	3.7		3.7	8.9	53.7	100.7	37	phenocryst interior
622-11913-2	3.9		3.9	8.8	54.3	102.4	36	phenocryst interior
622-11914-1	0.9		1.4	4.2	65.1	100.3	19	phenocryst interior
622-11914-2	0.9			4.2	65.8	98.6	17	phenocryst interior
622-11914-3	3.2		3.2	9.8	53.8	100.4	43	phenocryst margin
622-11914-4	1.3		1.4	4.2	64.8	100.4	22	phenocryst intermediate
622-11915-1	3.6		4.0	9.1	53.9	101.6	39	phenocryst interior
622-11915-2	2.9		3.3	11.6	54.4	103.3	53	phenocryst margin
622-11915-3	3.2		3.8	11.3	51.0	100.4	52	phenocryst outgrowth
622-11915-4	2.3		3.1	12.5	51.3	98.6	62	groundmass grain
622-11915-5	2.1		2.9	12.5	51.3	98.5	61	groundmass grain
622-11916-1	3.6		3.9	8.8	54.4	101.6	37	phenocryst interior
622-11916-2	4.1		3.8	8.7	53.3	100.7	35	phenocryst interior
622-11916-3	3.1		3.4	11.0	52.2	99.9	51	phenocryst margin
622-126161-3	3.7	0.35	3.1	11.1	51.1	99.4	48	see figure 2C
622-126161-6	4.0	0.43	2.9	11.3	51.0	100.1	48	see figure 2C
622-126161-7	3.7	0.38	2.4	11.5	51.6	98.7	46	see figure 2C
622-126161-8	3.4	0.41	3.2	11.0	49.6	97.2	50	see figure 2C
622-126162-5	2.3	0.42	1.2	13.5	52.1	98.5	61	see figure 2D
622-126162-6	2.4	0.43	1.8	11.8	53.6	99.7	53	see figure 2D
622-126163-5	2.6	0.46	1.4	14.1	52.4	100.7	63	see figure 2E
622-126163-6	2.3	0.51	1.1	13.5	53.5	100.3	60	see figure 2E

TABLE 5 (Continued)

Designation*	Mg**	Mn**	Al**	Ti**	Fe **	R_3O_4*** sum	Usp‡	Remarks
622-126163-7	1.1	0.46	2.4	5.6	60.7	99.2	26	see figure 2E
622-126163-8	1.4	0.49	2.4	5.7	60.7	99.8	26	see figure 2E
622-126163-9	2.2	0.54	0.9	14.6	52.1	99.6	65	see figure 2E
622-126164-3	2.6	0.47	1.5	13.0	52.4	99.4	58	see figure 2G
622-126164-4	2.6	0.44	1.9	12.5	52.5	99.5	56	see figure 2G
622-126164-6	2.3	0.45	1.6	11.6	53.9	99.0	52	see figure 2G
622-126164-7	2.5	0.47	1.2	13.0	52.0	98.2	59	see figure 2G
622-126164-9	2.3	0.41	1.1	13.1	53.2	99.5	59	see figure 2G
622-126151-5	2.2	0.47	1.3	12.6	52.8	98.3	57	see figure 2H
622-126151-6	2.2	0.49	1.6	12.4	52.4	98.2	57	see figure 2H
622-126151-8	2.2	0.43	1.8	11.6	53.2	98.2	54	see figure 2H
622-126151-9	2.2	0.49	1.4	12.7	52.1	97.8	59	see figure 2H
622-126152-1	2.9	0.33	4.1	7.0	54.2	98.2	31	see figure 2F
622-126152-2	4.1	0.31	2.7	12.3	49.0	98.3	54	see figure 2F
622-126152-3	3.8	0.31	2.0	13.4	48.5	97.5	60	see figure 2F
622-126152-4	3.8	0 39	1.7	14.2	48.2	97.6	63	see figure 2F
622-126152-9	4.0	0.31	2.0	13.2	49.3	98.6	57	see figure 2F
622-126152-10	3.8	0.25	3.5	10.4	50.6	98.7	46	see figure 2F
622-126152-11	3.2	0.27	4.0	7.5	54.8	100.2	32	see figure 2F
622-126153-6	2.2	0.41	1.2	12.7	52.9	98.1	57	see figure 2I
622-126153-7	2.1	0.45	1.6	11.6	54.0	98.8	53	see figure 2I
347-125141-6	4.1	0.34	2.5	14.1	48.2	99.7	63	see figure 2J
347-125141-7	4.2	0.32	2.4	13.9	48.3	98.4	63	see figure 2J
347-125141-8	4.1	0.34	3.2	11.7	50.2	100.2	50	see figure 2J
347-125141-9	4.2	0.30	3.5	11.8	50.1	100.9	51	see figure 2J
347-125141-12	4.0			13.7	49.8	96.1	56	see figure 2J
347-12521-3	4.2	0.32	4.5	7.2	53.3	100.3	27	see figure 2K
347-12521-4	4.0	0.30	4.4	7.0	53.5	99.9	26	see figure 2K
347-12531-2	1.5			14.6	52.0	95.8	68	see figure 2L
347-12531-3	1.5			15.0	51.5	95.9	70	see figure 2L
347-1-11	3.2	0.47	2.8	14.1	48.4	98.9	67	see figure 2M
347-1-12	3.1	0.44	3.0	14.0	48.3	99.0	67	see figure 2M
347-1-13	3.0			14.3	48.1	92.9	65	see figure 2M

* The two numbers following the specimen number refer to grain number and spot number.

** The values given are weight percents of the elements corrected as explained in the text (p. 706-708) and on tables 1 and 2.

*** The R_3O_4 sum is the weight sum of the oxide formulae as explained in the text (p. 706-708).

‡ The mole percent of Fe_2TiO_4 (Usp) is calculated as explained in the text (p. 706-708).

The petrography of iron-titanium oxide phenocrsysts in scoria is summarized in table 10. Most of the titaniferous magnetite and a large proportion of the ferrian ilmenite phenocrysts in the scoria specimens have been so extensively oxidized that further study was not warranted.

DISCUSSION

Estimation of the oxygen fugacity from the chemical compositions of titaniferous magnetite and ferrian ilmenite. The first task of this work is to establish the oxygen fugacity of alkaline basalt (at a known temperature). This is possible if titaniferous magnetite and ferrian-ilmenite have crystallized in equilibrium (Buddington and Lindsley, 1964).

TABLE 6

Analyses of titaniferous magnetite and ferrian-ilmenite across their contact

Designation*	Mg**	Mn**	Al**	Ti**	Fe **	R_2O_3*** sum	Usp‡	Distance from starting point and remarks
622-110113-0	2.9	(0.5)§	(1.3)§	12.2	53.2	99.7	52	see figure 2A near 622-110113-12
622-110113-20	2.9	(0.5)	(1.3)	13.1	52.9	100.4	52	+ 20 microns
622-110113-25	2.4	(0.5)	(1.3)	13.6	53.0	100.5	60	+ 25 microns
622-110113-28	2.7	(0.5)	(1.3)	14.9	50.1	98.7	71	+ 28 microns probably imperfect resolution
622-110113-30	2.8	(0.3)	(0.2)	25.6	38.0	sum R_2O_3*** 99.2	Hm†† 24	+ 30 microns probably imperfect resolution
622-11-113-32	3.3	(0.3)	(0.2)	28.4	34.3	99.1	15	+ 32 microns
622-110113-35	3.0	(0.3)	(0.2)	27.0	36.0	98.8	19	+ 35 microns
622-110113-40	2.5	(0.3)	(0.2)	25.6	38.1	98.8	23	+ 40 microns
622-110113-50	2.4	(0.3)	(0.2)	24.8	39.3	99.1	26	+ 50 microns
622-110113-60	2.2	(0.3)	(0.2)	24.5	39.9	98.4	27	+ 60 microns near 622-110113-1

* The two numbers following the specimen number refer to grain number and spot number.

** The values are weight percents of the elements corrected as explained in the text (p. 706-708) and on tables 1 and 2.

*** The R_2O_4 sum is the weight sum of the oxide formulae as explained in the text (p. 706-708).

‡ The mole percent of Fe_2TiO_4 (Usp) is calculated as explained in the text (p. 706-708).

§ The values in parentheses are assumed on the basis of nearby analyses.

†† The mole percent of Fe_2O_4 (Hm) is calculated as explained in the text (p. 706-708).

TABLE 7

Analyses of ferrian ilmenite integrown with titaniferous magnetite in trachybasalt

Designation*	Mg**	Mn**	Al**	Ti**	Fe**	R_2O_3*** sum	Hm‡	Remarks
622-110113-1	2.1	0.34	0.26	24.8	40.2	99.8	26	see figure 2A
622-110113-2	2.6		0.24	24.9	39.4	98.6	26	see figure 2A
622-110113-3	2.9		0.18	27.1	36.1	96.9	17	see figure 2A
622-110113-4	2.4		0 3	24.9	39.3	99.0	25	see figure 2A
622-110113-5	2.5		0.4	24.8	39.1	98.8	26	see figure 2A
622-110113-6	3.1		0.16	28.0	34.8	98.4	15	see figure 2A
622-110113-7	2 3		0.3	25.0	38.8	98.2	24	see figure 2A
622-110113-8	2.3		0.25	24.8	39.4	98.0	25	see figure 2A
622-110113-9	3.2		0.20	27.5	35.4	98.7	18	see figure 2A
622-11911-1	4.5		0.17	29.8	30.9	98.0	12	see figure 2B
622-11911-2	4.4		0.17	29.2	31.5	97.7	14	see figure 2B
622-11911-1′	4.9			28.5	30.8	96.7	17	repeat of 1

TABLE 7 (Continued)

Designation*	Mg**	Mn**	Al**	Ti**	Fe**	R_2O_3*** sum	Hm††	Remarks
622-11911-2′	4.7			28.5	31.4	97.0	17	repeat of 2
622-126161-1	4.6	0.32	0.33	28.5	33.5	100.9	20	see figure 2C
622-126161-2	4.9	0.41	0.26	29.7	31.9	100.5	16	see figure 2C
622-126161-4	4.8	0.35	0.21	29.7	31.1	99.5	14	see figure 2C
622-126161-5	4.4	0.33	0.32	28.6	33.6	100.9	19	see figure 2C
622-126162-1	2.1	0.30	0.53	25.5	40.2	101.4	24	see figure 2D
622-126162-2	2.2	0.31	0.29	25.6	40.0	100.7	24	see figure 2D
622-126162-3	2.7	0.34	0.28	27.2	37.4	100.7	20	see figure 2D
622-126162-4	2.7	0.38	0.15	28.3	35.9	100.1	15	see figure 2D
622-126163-1	1.9	0.29	0.33	24.1	41.9	100.9	28	see figure 2E
622-126163-2	2.2	0.33	0.27	24.9	39.9	99.8	25	see figure 2E
622-126163-3	2.9	0.42	0.18	28.4	36.0	100.8	16	see figure 2E
622-126163-4	3.4	0.43	0.15	29.5	33.6	99.9	12	see figure 2E
622-126164-1	2.4	0.30	0.30	25.2	40.6	101.4	27	see figure 2G
622-126164-2	2.8	0.36	0.27	27.1	36.2	98.9	19	see figure 2G
622-126164-8	2.8	0.46	0.22	28.1	34.6	98.4	14	see figure 2G
622-126164-10	2.2			24.9	39.3	97.6	24	see figure 2G
622-126151-1	2.0	0.29	0.29	24.9	39.8	99.3	24	see figure 2H
622-126151-2	2.2	0.29	0.25	25.0	39.5	99.2	25	see figure 2H
622-126151-3	2.6	0.36	0.21	27.6	35.5	98.1	16	see figure 2H
622-126151-4	2.8	0.43	0.17	27.6	36.2	99.6	18	see figure 2H
622-126151-7	2.6	0.46	0.24	28.0	35.0	98.5	14	see figure 2H
622-126152-5	4.0	0.22	0.36	27.8	33.2	98.4	18	see figure 2F
622-126152-6	3.9	0.23	0.57	26.6	34.8	98.9	23	see figure 2F
622-126152-7	3.9	0.17	0.48	26.3	35.6	99.5	25	see figure 2F
622-126152-8	4.0	0.29	0.30	28.3	32.7	98.2	16	see figure 2F
622-126153-1	2.0	0.30	0.25	25.0	40.1	99.9	25	see figure 2I
622-126153-2	1.9	0.32	0.25	24.8	39.9	99.0	24	see figure 2I
622-126153-3	2.2	0.34	0.23	26.5	37.7	99.0	19	see figure 2I
622-126153-4	2.5	0.38	0.18	27.3	37.0	99.7	18	see figure 2I
622-126153-5	2.9	0.45	0.15	28.6	34.6	99.2	14	see figure 2I
347-1-8	4.5	0.43	0.08	31.3	29.1	98.2	6	see figure 2M
347-1-9	4.5			30.3	30.0	97.2	9	see figure 2M
347-1-10	4.2			30.3	30.4	97.9	8	see figure 2M
347-1-14	4.4	0.45	0.08	31.0	29.4	98.2	6	see figure 2M
347-125151-1	5.5		0.25	30.6	29.7	99.9	13	see figure 2J
347-125141-2	5.2			30.4	29.2	97.8	11	see figure 2J
347-125141-3	5.8			30.9	28.6	99.0	12	see figure 2J
347-125141-4	5.9	0.31	0.14	31.3	28.1	99.8	11	see figure 2J
347-125141-5	5.3			30.3	29.8	98.7	13	see figure 2J
347-125141-10	5.2			25.2	35.1	98.3	28	see figure 2J
347-125141-11	6.2			31.7	27.3	98.9	9	see figure 2J
347-12521-1	5.9	0.30	0.19	29.9	28.0	97.5	14	see figure 1K
347-12521-2	6.7	0.34	0.16	30.0	28.1	98.6	19	see figure 1K
347-12531-1	2.2			29.8	31.9	94.4	3	see figure 1L

* The two numbers following the specimen number refer to grain number and spot number.

** The values are weight percents of the elements corrected as explained in the text (p. 706-708) and on tables 1 and 2.

*** The R_2O_3 sum is the weight sum of the oxide formulae as explained in the text (p. 706-708).

†† The mole percent of Fe_2O_3 (Hm) is calculated as explained in the text (p. 706-708).

Phenocrysts of titaniferous magnetite, which are intergrown with ferrian-ilmenite, vary in composition in the two trachybasalt specimens 622 and 347. Where, if at all, has equilibrium been attained? What is the meaning of the compositional variation of the oxide phenocrysts? These questions are best considered in terms of the ternary phase diagram for the system FeO + Fe_2O_3 + TiO_2 which is shown on figure 1 (Webster and Bright, 1961; Taylor, 1964).

Figure 1 depicts the phases stable at a fixed temperature (1200°C) but variable oxygen fugacities and bulk compositions. The line W-A′-B-C′-D-E′-F-TiO_2 is a diagrammatic oxygen fugacity isobar. Compositions lying on the line W-A′ consist of mixtures of wustite of composition W and titaniferous magnetite of composition A′. Bulk compositions falling on the line A′-B consist of a single phase corresponding to the bulk composition. At the given temperature and oxygen fugacity a series of titaniferous magnetites is stable extending from A′ to B. The titaniferous

TABLE 8

Analyses of titaniferous magnetite in trachyandesites, 572, 486, 491, 68, and trachyte, 560

Designation*	Mg**	Mn**	Al**	Ti**	Fe **	R_2O_3*** sum	Usp‡	Remarks
572-1-1	1.1	1.1	0.8	8.6	58.0	97.9	39	phenocryst interior
572-1-2	1.1	1.3	0.9	9.1	59.2	100.3	40	phenocryst margin
572-2-1	1.6	1.3	0.9	9.2	58.6	100.6	38	phenocryst interior
572-2-2	1.0	1.1	1.0	8.7	58.8	99.3	40	phenocryst margin
486 mt[a]	2.1		1.4	9.3	56.8	98.5	41	phenocryst 30μ from ilmenite
486 mt[b]	2.1		2.2	8.0	57.9	99.5	36	average of 7 interiors of euhedral phenocrysts
491 mt[a]	2.1		2.1	7.8	57.4	98.3	35	average of 5 interiors of euhedral phenocrysts
491 mt[b]	1.3		1.3	5.4	62.2	98.3	24	average of 2 interiors of rounded phenocrysts
68 mt[a]	2.2		2.3	7.8	57.7	99.4	35	average of 4 interiors of euhedral phenocrysts
68 mt[b]	1.6		1.4	5.5	62.2	99.5	23	rounded phenocryst
560-1-2	0.9	1.2	0.3	10.3	56.2	96.7	47	phenocryst lamella
560-1-3	1.1	1.2	0.3	11.0	54.8	96.1	51	phenocryst interior
560-1-6	1.0	1.4	0.3	11.1	58.0	100.3	49	phenocryst margin
560-2-1	1.2	1.4	0.7	9.0	57.6	98.0	39	phenocryst interior
560-2-2	1.1	1.7	0.4	10.8	55.7	98.0	48	phenocryst intermediate
560-2-3	1.2	1.2	0.6	10.0	57.8	99.8	44	phenocryst margin

* The two numbers following the specimen number refer to grain number and spot number.

** The values given are weight percents of the elements corrected as explained in the text (p. 706-708) and on tables 1 and 2.

*** The R_3O_4 sum is the weight sum of the oxide formulae as explained in the text (p. 706-708).

‡ The mole percent of Fe_2TiO_4 (Usp) is calculated as explained in the text (p. 706-708).

TABLE 9

Analyses of ferrian ilmenite phenocrysts

Designation*	Mg**	Mn**	Al**	Ti**	Fe**	R_2O_3*** sum	Hm‡	Remarks
560-1-1	1.5	1.0	0.03	24.5	38.2	95.8	23	phenocryst interior
560-1-5	2.0	1.8		28.8	33.3	97.3	10	phenocryst lamella
486-ila	2.5		0.3	25.2	38.3	97.6	24	average of interiors of 2 phenocrysts
486-ilb	2.6		0.3	25.2	38.6	97.3	24	phenocryst 30μ from mt
491-il	2.6		0.3	25.2	38.6	97.3	24	phenocryst interior

* The two numbers following the specimen number refer to grain number and spot number.

** The values given are weight percents of the elements corrected as explained in the text (p. 706-708) and on tables 1 and 2.

*** The R_3O_4 sum is the weight sum of the oxide formulae as explained in the text (p. 706-708).

‡ The mole percent of Fe_2O_3 (Hm) is calculated as explained in the text (p. 706-708).

TABLE 10

Petrography of iron-titanium oxide phenocrysts in scoria

Specimen number	Location	Appearance of specimen	Notes on oxide phenocrysts*
56	Hillpiece	brownish-gray scoria	Ti-mt and il-mt
133	Halfway Beach	red cinder	Ti-hm, rt, psb, relict Ti-mt
144	The Knobs (western flank)	gray scoria	il-mt
160	First Lagoon Gulch (sea level)	red cinder	il-mt, minor psb, rt
235	Hill-with-a-hole-in scoriaceous top to trachyandesite lava	gray scoria	Ti-mt
356	Main crater 6500 ft. elevation	gray scoria	Ti-mt containing unoxidized pyrrhotite inclusions

* Abbreviation are as follows: Ti-mt = homogeneous titaniferous magnetite, il-mt = ilmeno-magnetite, Ti-hm = titaniferous hematite, rt = rutile, psb = pseudo-brookite.

magnetite at A′ (in equilibrium with wustite) is poor in oxygen (R_2O_3) and poor in titanium. Toward B the stable titaniferous magnetites become richer in both titanium and oxygen. Similar relationships hold for ferrian-ilmenite along the line C′-D, progressing from C′ (in equilibrium with titaniferous magnetite) to D (in equilibrium with ferro-pseudo-brookite) the ferrian-ilmenite becomes richer in oxygen (R_2O_3) and richer in titanium. The composition of either titaniferous magnetite or ferrian-ilmenite can vary widely, even if the temperature and oxygen fugacity are constant.

Only if titaniferous magnetite and ferrian-ilmenite are in equilibrium are their respective compositions fixed uniquely. In a basaltic magma the temperature and particularly the oxygen fugacity and TiO_2 activity may vary from one place to another. Consequently, it is not safe to assume that separate crystals of the iron-titanium oxides have crystallized under identical conditions. Only at the interface between titaniferous magnetite and ferrian-ilmenite can mutual saturation and reaction be assumed.

Two conditions must be met, if the oxygen fugacity and temperature of the basaltic liquid can be deduced from the compositions of titaniferous magnetite and ferrain ilmenite at their contact. These conditions are: (1) equilibrium between magnetite and ilmenite must be established at their contact, and (2) this equilibrium must correspond to conditions in the melt some distance away from the grain boundary. In the present case it is not possible to *prove* that either of these conditions are met.

The first condition is assumed because all constituents are available at the grain boundary which make possible the exchange reaction: $Fe_2TiO_4 + Fe_2O_3 = FeTiO_3 + Fe_3O_4$. In other words, heat is the only item which must be communicated externally in order to attain equilibrium at the contact.

A necessary, but insufficient, test of the second condition is that the compositions of ferrian ilmenite and titaniferous magnetite are constant along their contact within each grain and from one grain to another. Figures 2 and 4, and table 11, reveal that variation exists which exceeds the analytical precision and amounts to about ± 2 percent Hm and

TABLE 11

Summary of results on Tristan da Cunha lavas

Designation	Usp	Hm	T°C	$-\log_{10}f_{O_2}$	Remarks
622-12616-1	48	14	990	10.4	grain surrounded by groundmass
622-12616-2	61	15	1130	8.7	half ilmenite and half magnetite
622-12616-3	65	12	1090	9.5	mostly magnetite
622-12616-4	59	14	1090	9.2	mostly ilmenite
622-12615-1	59	14	1090	9.2	mostly ilmenite
622-12615-2	63	16	1160	8.3	polycrystalline fragment
622-12615-3	57	14	1070	9.5	mostly ilmenite
622-11011-3	62	15	1130	8.7	mostly magnetite
622-1191-1	63	15	1140	8.6	mostly magnetite
347-12514-1	63	11	1070	9.8	mostly magnetite
347-1252-1	26	14-19	850	12.0	in augite with FeO(OH)
347-1253-1	69	3	890	13.8	groundmass magnetite and ilmenite
347-1	67	6	990	11.4	mostly magnetite
486	41	24	1110*	7.8*	two nearby phenocrysts
560	47	10	930	11.7	lamellar intergrowth

* Deduced by extrapolation of the data of Buddington and Lindsley (1964) and Taylor (1964).

± 8 percent Usp. This variation corresponds to a range in temperature from 990°C to 1160°C and in oxygen fugacity from $10^{-10.4}$ to $10^{-8.3}$ bars. In contrast the Usp content of the margins of the titaniferous magnetite phenocrysts is practically uniform within analytical precision and equals 52 ± 2. The variation at the ilmenite-magnetite contact is due to lack of complete equilibrium attainment between the phenocrysts and the liquid, probably just prior to or during eruption. Since the Fe_2O_3/FeO ratios of both ferrian ilmenite and titaniferous magnetite

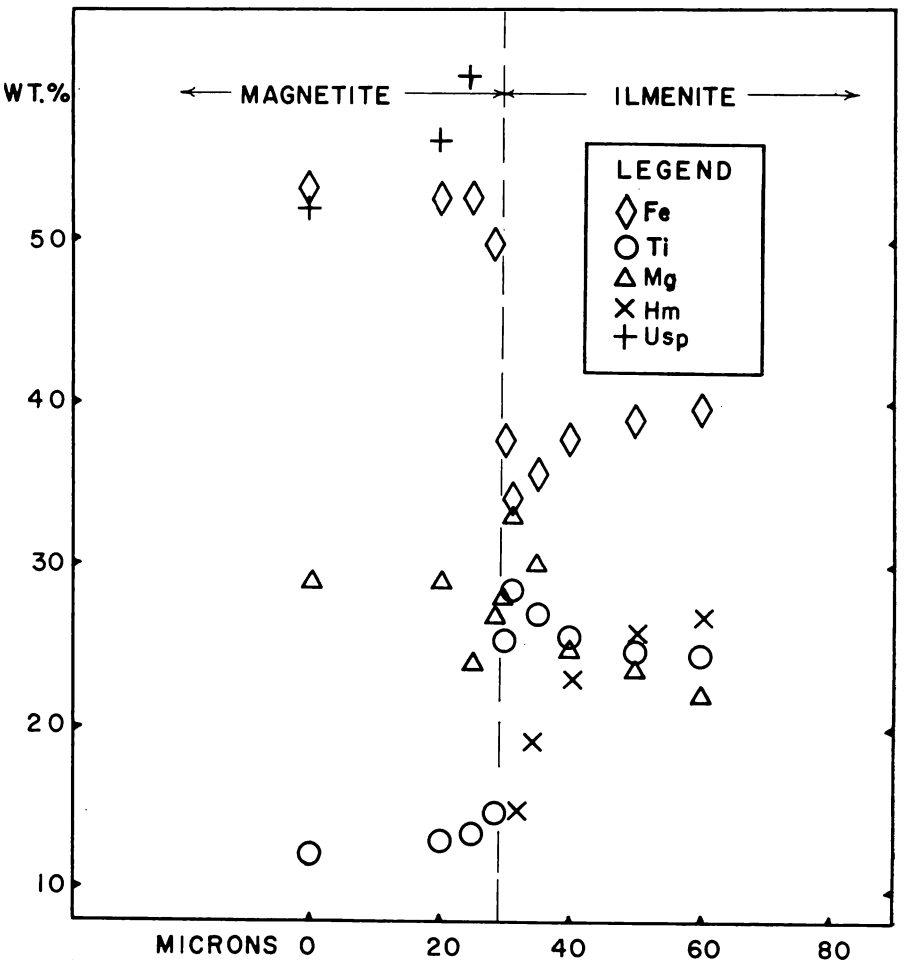

Fig. 3. Compositional variation of intergrown titaniferous magnetite and ferrian ilmenite across their contact. The plotted values are given in table 6. Usp and Hm are plotted as mole percents. Note the increase in Ti content of ferrian ilmenite as the contact with titaniferous magnetite is approached. Since the magnetite is relatively poor in Ti, this trend cannot be due to an analytical artifact produced by the proximity to the grain boundary. Note that Usp *increases* as the ferrian ilmenite is approached. If ferrian ilmenite were produced by oxidation of titaniferous magnetite, Usp would have to decrease to maintain material balance.

decrease toward their contact, the phenocrysts are being reduced by the liquid. Consequently, if equilibrium with the melt is being approached, the deduced oxygen fugacities are maximal for the indicated temperatures.

The change in composition of the iron-titanium oxide phenocrysts away from their mutual grain boundary (fig. 3) indicates disequilibrium in terms of oxygen fugacity, TiO_2 activity, or both, if the temperature is constant. If stable equilibrium exists at the grain boundary, then the decrease in Hm toward the grain boundary signifies a decrease in oxygen fugacity. The activity of TiO_2 may increase or decrease depending on the (unknown) trend of isoactivity lines for TiO_2 in the one phase, ferrian ilmenite field and how the cation to oxygen ratio of the ilmenite changes. The increase in Usp near the boundary also can be due to a decrease in the oxygen fugacity. However, the unknown cation to oxygen ratio of the titaniferous magnetite permits the possibility that the increase in Usp is solely due to an increase in the activity of TiO_2. If, as seems plausible, isoactivity lines for TiO_2 in the one phase fields are approximately parallel to lines of constant TiO_2 content, then gradients in activity of TiO_2 as well as oxygen fugacity existed in the composite phenocrysts under isothermal conditions.

The textures and compositional relations of the iron-titanium oxide phenocrysts suggest that Fe_2O_3-rich ferrian ilmenite is an unstable mineral in the trachybasalt liquid. The ferrian ilmenite in the trachybasalt specimens 622 and 347 is in no case in direct contact with groundmass or glass but is invariably separated from it by titaniferous magnetite or augite. Lamellae of titaniferous magnetite occur in the ferrian ilmenite and are similar to the lamellae formed parallel to the basal plane by experimental reduction of ferrian ilmenite (Lindsley, written commun., 1967). Toward titaniferous magnetite the Hm content of the ferrian ilmenite decreases indicating partial adjustment to relatively reducing conditions. Probably the ferrian ilmenite was introduced into the trachybasalt magma as xenocrysts or as phenocrysts inherited from a more oxidized magma. Prior to and during eruption the ferrian-ilmenite reacted with the trachybasalt magma which was relatively reducing and probably also at a relatively low TiO_2 activity. Titaniferous magnetite grew as a product of reduction of the ferrian ilmenite and the liquid gained TiO_2 according to a reaction such as: $(Fe_2O_3 + 3FeTiO_3)$ ferrian ilmenite $= (Fe_2TiO_4 + Fe_3O_4)$ titaniferous magnetite $+ (2TiO_2)$ liquid.

Oxygen fugacities and temperatures were deduced from the compositions of adjacent (within 10 microns) titaniferous magnetite and ferrian ilmenite. The results, which are for two trachybasalts, one trachyandesite, and one trachyte, are summarized in table 11 and plotted on figure 4. For both trachybasalts the range of oxygen fugacities and temperatures is due to different results obtained on different grains. The disparity of results obtained for different grains seem beyond analytical precision (see above, page 718) and is probably due to lack of equilibrium attainment with the liquid prior to eruption. Thus the data delimit

rather than define the oxygen fugacity of the liquid. For a reference, a straight line was fitted to the data. The original temperature and oxygen fugacity of the trachybasalt magmas was probably below but close to the lines for specimens 622 and 347, because the ferrian ilmenite was being reduced by the magma.

The effect of crystallization on the oxygen fugacity. I wish to relate the oxygen fugacities of the Tristan lavas to each other and to those of other rocks in terms of oxidation-reduction reactions with an external environment and in terms of the conditions at the site of magma generation. To do this it is necessary to estimate the effect of crystallization on the oxygen fugacity. Such an estimate is attempted in the following section.

The variation of oxygen fugacity and temperature due to igneous crystallization can be considered in terms of the role played by ferrous and ferric iron in the magma. For example, the oxygen fugacity of a silicate melt can be related to the temperature and the ratio of the activities of ferric and ferrous iron according to the following reaction and equilibrium constant, Fudali, 1965):

$$4FeO \text{ (in silicate melt)} + O_2 = 4FeO_{1.5} \text{ (in silicate melt)} \quad (1)$$

$$K_T = [(a\ FeO_{1.5})^4/(a\ FeO)^4]f_{o_2}^{-1} \quad (2)$$

The activities (a) are related to molar concentrations (X) by activity coefficients (γ) so that:

$$K_T = \left[\frac{(\gamma FeO_{1.5})^4(X\ FeO_{1.5})^4}{(\gamma FeO)^4(X\ FeO)^4}\right] f_{o_2}^{-1} \quad (3)$$

Consequently the oxygen fugacity of a silicate melt can be expressed as the product of three terms:

$$f_{o_2} = \frac{(1)}{(K_T)} \cdot \frac{(X\ FeO_{1.5})^4}{(X\ FeO)^4} \cdot \frac{(\gamma FeO_{1.5})^4}{(\gamma FeO)^4} \quad (4)$$

Changes in each of these factors due to crystallization of basaltic liquid are considered below.

1. The equilibrium constant (first factor) will be affected by the temperature. Thermodynamics requires that $\log K_T = C/T + B$ with $C = \Delta H/2.303R$. Furthermore $d(\log K)/d(1/T) = C$. If the ratio of the activities of $FeO_{1.5}$ and FeO remains constant, then $d(\log K) = -d(\log f_{o_2})$ and $-d(\log f_{o_2}) = C\ d(1/T)$. Since C is a constant $(\log f_{o_2})_1 - (\log f_{o_2})_2 = C\ [(1/T)_1 - (1/T)_2]$. Values of C can be deduced from the data of Darken and Gurry (1946). Reading their figure 3B at $N_2/N_1 = 1.1$ (that is, $FeO_{1.5}/FeO = 0.125$) gives $C = -29 \times 10^3$ for 1600°C to 1500°C and $C = -30 \times 10^3$ for 1500°C to 1400°C. A value of C can similarly be deduced from the data of Shibata (1967) on a natural basaltic liquid. Reading Shibata's figure 3 at $\log FeO/FeO_{1.5} = 0.75$ yields $C = -28 \times 10^3$ for 1300°C to 1200°C.

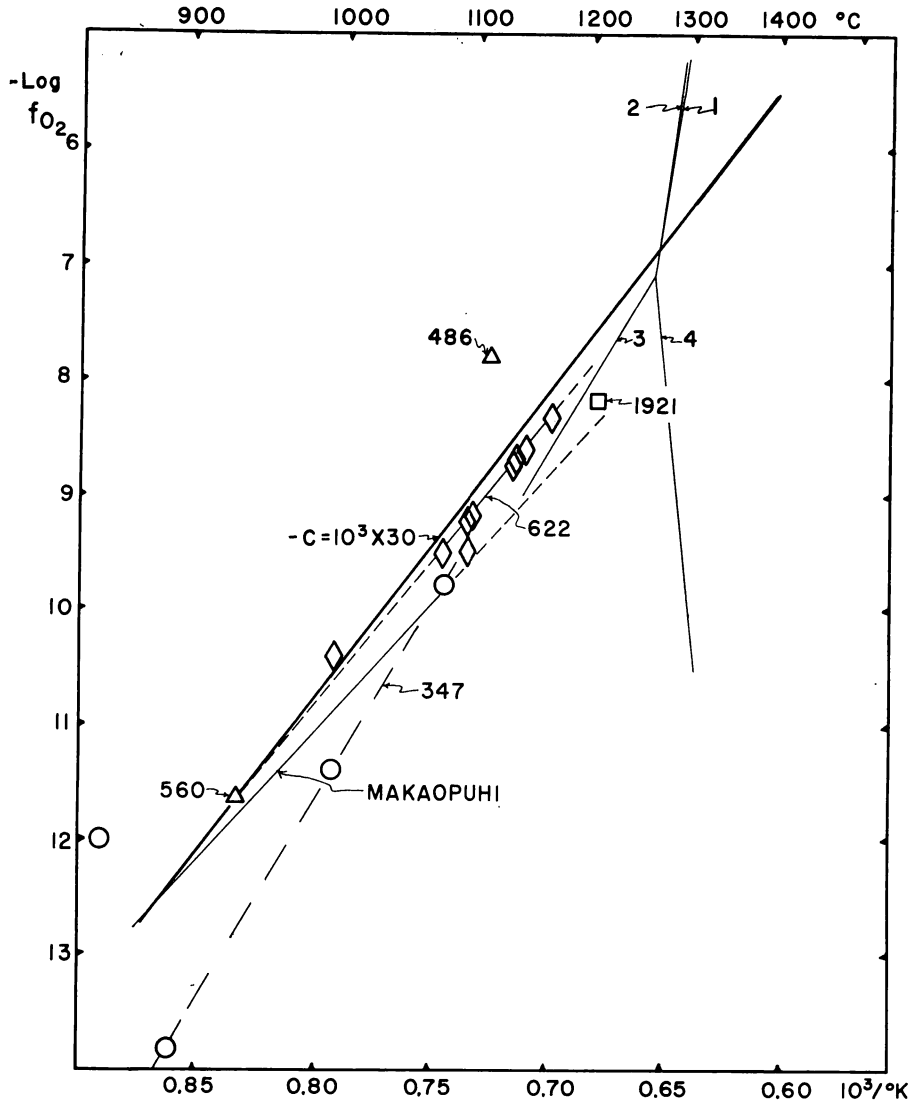

Fig. 4. The oxygen fugacity and temperature relations of trachybasalt and other lavas, Tristan da Cunha. The new data for Tristan trachybasalts (622) and (347), trachyandesite (486), and trachyte (560) are from table 11. The lines drawn through the several points for (622) (diamonds) and (347) (circles) correspond to the respective equations:

$$\log f_{o_2} = 9.0 - 24.9 \frac{1000}{T°K} \text{ and } \log f_{o_2} = 15.8 - 34.4 \frac{1000}{T°K}$$

The line designated Makaopuhi is that of equation 9 found by Sato and Wright (1966) for a subalkaline basaltic lava lake at Kilauea volcano, Hawaii. The square designated 1921 is the oxygen fugacity of subalkaline basalt of Kailauea volcano erupted in 1921 which was determined by Fudali (1965) at 1200°C. The reference line marked

Other data (Kennedy, 1948; and Fudali, 1965) give values of C close to -20×10^3. But Kennedy's data are for 0.2 atm oxygen fugacity, and Fudali gives only two points (1200°C, log $f_{o_2} = -6.4$, and 1150°C, log $f_{o_2} = -6.9$). The agreement between the more extensive data of Darken and Gurry and Shibata suggests that a slope of about $-30 \times 10^3 = d(\log f_{o_2})/d(1/T)$ is preferable until more data are available. For these reasons a reference line with the slope of $C = -30 \times 10^3$ is drawn on figure 4. The slope of this reference line represents the expected change in oxygen fugacity for a given change in temperature with the ratio of the activities of $FeO_{1.5}$ and FeO held constant. Deviations from this slope thus may be interpreted in terms of changes in the ratio of the activities of $FeO_{1.5}$ and FeO.

2. The molecular ratio of Fe_2O_3/FeO (= 1/2 $FeO_{1.5}/FeO$) in the liquid may change with crystallization owing to any inequal distribution of ferric and ferrous iron between crystals and liquid. Conceivably the Fe_2O_3/FeO ratio could also be affected by other redox buffers such as H_2/H_2O, Mn^{+3}/Mn^{+2}, CO/CO_2, et cetera. Relative to the usual abundance of ferric iron (about 1 wt percent Fe_2O_3), the gaseous constituents have little leverage in a near surface environment because of low solubility. The abundance of manganese is generally an order of magnitude lower than that of ferric iron. Throughout the range of crystallization over which the liquid has a basaltic composition iron oxide is the buffer that controls the oxygen fugacity.

In a crystallizing basaltic liquid, the fractionation of ferric and ferrous iron will be largely governed by the relative proportions of iron-titanium oxides and ferromagnesian silicates. The data of Sato and Wright (1966) and Fudali (1965) in conjunction with that of Buddington and Lindsley (1964) indicate that the Fe_2O_3/FeO ratios of iron titanium oxides in basalts may range from 0.1 to 0.25 for ilmenites and from 0.1 to 0.37 for magnetites. For ferromagnesian silicates this ratio ranges from less than 0.01 for olivines to 0.03 for orthopyroxenes to 0.1 for augites. Chromites with a molecular ratio of $Fe_2O_3/FeO \approx 0.2$ probably have negligible influence because of their low abundance.

To a first approximation it is the proportion of olivine plus orthopyroxene to iron-titanium oxides that establishes the Fe_2O_3/FeO ratio of the crystals. Considering the range in molecular Fe_2O_3/FeO ratios of fresh basalts to be from 0.05 to 0.15, it is apparent that only if the proportion of olivine plus orthopyroxene to oxide falls substantially below 2, can the Fe_2O_3/FeO ratio of the liquid significantly decrease

---

$-C = 10^3 \times 30$ is deduced from the data of Darken and Gurry (1946) and Shibata (1967) as discussed in the text (p. 721). The lines numbered 1 to 4 are for the following univariant assemblages in the system MgO + FeO + Fe_2O_3 + SiO_2 (Muan and Osborn, 1956):

1. = magnesioferrite + olivine + pyroxene + liquid;
2. = magnesioferrite + pyroxene + tridymite + liquid;
3. = magnesioferrite + olivine + tridymite + liquid;
4. = olivine + pyroxene + tridymite + liquid.

as a result of crystallization. In general a moderate increase will be expected. For example: the calculated effect of fractional crystallization of 20 weight percent of olivine (Fa 20) from an original liquid having 10 weight percent FeO and 1.8 weight percent Fe_2O_3 is to increase the molecular ratio of Fe_2O_3/FeO by a factor of about 1.5. If this change were to occure isothermally, the oxygen fugacity would increase approximately one order of magnitude (compare Fudali, 1965, fig. 3).

The system MgO + FeO + Fe_2O_3 + SiO_2 (Muan and Osborn, 1956) illustrates the opposing effects of crystallization of oxide-bearing univariant assemblages (curves 1-3, fig. 4) compared to a univariant assemblage lacking an oxide (curve 4, fig. 4). In natural basalts the presence of titanium permits the oxide to have a relatively low Fe_2O_3/FeO ratio, hence the crystallization of an oxide phase in basalt does not as drastically alter the Fe_2O_3/FeO ratio of the residual liquid as it would in a TiO_2-free system.

The stage of crystallization at which an iron-titanium oxide commences to crystallize varies. The first iron-titanium oxide mineral to appear during crystallization of Hawaiian subalkaline basalt is ferrian-ilmenite (Wright and Weiblen, 1967). It appears at about 1070°C and after about 50 percent of crystallization (Peck, Wright, and Moore, 1966; Häkli and Wright, 1967; Wright and Weiblen, 1967). It is joined by titaniferous magnetite at about 1050°C and after about 65 percent solidification (Wright and Weiblen, 1967). In contrast, alkaline basalts with a relatively high TiO_2/(FeO + Fe_2O_3) ratio and a low silica activity generally crystallize titaniferous magnetite at a relatively early stage. This follows from the application of the mass action law to the two reactions:

1. $Fe_2SiO_4 + TiO_2 = Fe_2TiO_4 + SiO_2$
2. $3Fe_2SiO_4 + O_2 = 2Fe_3O_4 + 3SiO_2$.

At equivalent stages of crystallization, the crystals growing from an alkaline basalt are likely to have a higher Fe_2O_3/FeO ratio compared to the liquid than are those growing from subalkaline basalt. Thus the oxygen fugacity of an alkaline basalt may be expected to decrease somewhat more rapidly with advancing crystallization than that of a subalkaline basalt.

3. Variation in ($\gamma FeO_{1.5}$)/(γFeO) during crystallization is difficult to predict. Calculations based on experiments with metallurgical systems suggest that the basicity (for example, activity of O^{-2} ion) of the melt may exert an important influence on the ($\gamma FeO_{1.5}$)/(γFeO) ratio, particularly at iron concentrations below 25 mole percent (Larson and Chipman, 1953). In the system: CaO + SiO_2 + FeO + Fe_2O_3, a decrease in the CaO/SiO_2 ratio from 1.3 to 0.54 results in an increase of the oxygen fugacity of about two orders of magnitude, if the bulk composition contains 20 mole percent FeO + Fe_2O_3 and if temperature and Fe_2O_3/FeO remain constant. The early crystallization of a basaltic magma generally depletes the liquid in CaO and MgO but enriches it

in Na_2O and K_2O. These two results will have opposing influence on the basicity of the melt and presumably on the ratio of $(\gamma FeO_{1.5})/(\gamma FeO)$ (Paul and Douglas, 1965; Carmichael and Nicholls, 1967). Further experiments are required in order to establish which effect will predominate in basaltic liquids.

4. Summary of the effect of crystallization on the oxygen fugacity. The principal factors, which are internally defined, and which govern the oxygen fugacity of a crystallizing basalt magma are its temperature and composition. Of these temperature predominates. Consequently the oxygen fugacity + temperature pairs for the 4 Tristan lavas summarized in table 11 and figure 4 can be directly compared with similar data on other lavas of different composition.

The origin of the oxygen fugacity of Tristan trachybasalt. I have argued above that temperature is likely to exert the dominant influence on the oxygen fugacity of a basalt magma. This argument is supported by the close parallelism between the oxygen fugacity-temperature curves, which are shown on figure 4, for the crystallization of subalkaline basalt (Sato and Wright, 1966), alkaline basalt (trachybasalt specimens 622 and 347), and for the behavior of pure iron oxide melt (Darken and Gurry, 1946) as well as basalt liquid (Shibata, 1967). The slopes of the curves for Tristan alkaline basalt are slightly steeper than that for Hawaiian subalkaline basalt. This is the anticipated result due to the relatively early appearance of titaniferous magnetite and the relatively low content of olivine in the Tristan basalts.

The Mg and Hm contents of the ferrian-ilmenite in trachybasalt overlap those of phenocrysts in trachyandesites and trachyte. As can be seen on figure 4, the oxygen fugacity of the trachyandesite (specimen 486) is too high to be the result of any of the internally controlled processes of crystallization discussed above. It is possible that the observed oxygen fugacity of Tristan alkaline basalt has been affected by admixture with oxidized residual liquid or solid.

Whereas the Tristan data reflect intratelluric conditions, the Hawaiian data are for erupted materials. At present it is difficult to assess any changes which the Hawaiian basalts may have endured due to loss of juvenile gas or admixture of atmospheric gases during eruption. The intratelluric crystallization conditions of two Kilauean (Hawaii) subalkaline basalts which contain iron-titanium oxide phenocrysts were more highly oxidizing than those of eruption (Anderson, 1968). This result closes the already small gap between the oxygen fugacities of Hawaiian subalkaline basalt and Tristan alkaline basalt. In conclusion, the difference between the oxygen fugacity of Tristan alkaline basalt liquid and Hawaiian subalkaline basalt liquid is probably less than 0.3 log units at 1200°C.

Although the oxygen fugacities of Tristan trachybasalt specimens 622 and 347 differ by only a small factor from those of Hawaiian subalkaline basalt (Fudali, 1965; Sato and Wright, 1966), the ratio of Fe_2O_3/FeO in the trachybasalts (622 = 0.14, 347 = 0.24) is consider-

ably greater than it is in Hawaiian subalkaline basalt (0.09) (Baker and others, 1964; Fudali, 1965). The differences in Fe_2O_3/FeO ratios corresponds to an expected difference in oxygen fugacity of more than one order of magnitude (see, for example, Fudali, 1965, fig. 3). This expected difference is not observed. Presumably the higher Fe_2O_3/FeO ratio of the trachybasalt magma is compensated by other compositional factors, particularly its higher basicity.

If alkaline basalt (such as Tristan trachybasalt) is derived from subalkaline basalt by processes that include gas transfer and oxidation (Engel, Engel, and Havens, 1965), then the present data suggest that oxidation is coincidentally compensated by increased melt basicity such that a nearly equivalent oxygen fugacity is maintained. On the other hand, if alkaline basalt magma is generated at a greater temperature and pressure than is subalkaline basalt magma (Yoder and Tilley, 1962), then the near identity of oxygen fugacities suggests that the oxygen fugacity is buffered by phases of similar composition in both environments of origin. Olivine, chromite, and pyroxene could provide a suitable buffer according to: $3Fe_2SiO_4$ (solid solution in olivine) + $1/2\ O_2$ = Fe_3O_4 (solid solution in chromite) + $3FeSiO_3$ (solid solution in pyroxene).

ACKNOWLEDGMENTS

I am idebted to R. L. Smith, U.S. Geological Survey, for recommending the Tristan rocks for study, to I. G. Gass, Leeds University, England, for generous donation of specimens, and to P. B. Barton, D. R. Wones, B. C. Hearn, and T. L. Wright, U. S. Geological Survey, and N. D. Watkins, Florida State University, for helpful discussion and criticism. D. H. Lindsley, Geophysical Laboratory, and P. B. Barton critically reviewed the manuscript and made particularly helpful suggestions. H. J. Rose, Jr., U. S. Geological Survey, and K. Fredericksson, Smithsonian Institution, kindly permitted me to use their microprobes. Use of sample preparation and photographic facilities of E. Roedder, U. S. Geological Survey, is greatly apreciated.

REFERENCES

Anderson, A. T., 1968, Reduction of iron-titanium oxide phenocrysts during eruption of alkaline and subalkaline basaltic magmas [abs.]: Am. Geophys. Union, Trans., v. 49, p. 352.

———— in press, Oxidation of the La Blache Lake titaniferous magnetite deposit, Quebec: Jour. Geology, v. 76, p.

Baker, P. E., Gass, I. G., Harris, P. G., and Le Maitre, R. W., 1964, The volcanological report of the Royal Society expedition to Tristan da Cunha, 1962: Royal Soc. London, Philos. Trans., ser. A., Math. Phys. Sci., v. 256, p. 439-578.

Buddington, A. F., Fahey, J., and Vlisidis, A., 1963, Degree of oxidation of Adirondack iron oxide and iron-titanium oxide minerals in relation to petrogeny: Jour. Petrology, v. 4, p. 138-169.

Buddington, A. F., and Lindsley, D. H., 1964, Iron-titanium oxide minerals and synthetic equivalents: Jour. Petrology, v. 5, p. 310-357.

Carmichael, I.S.E., 1967, The iron-titanium oxides of salic volcanic rocks and their associated ferromagnesian silicates: Beitr. Mineralogie Petrologie, v. 14, p. 36-64.

Carmichael, I. S. E. and Nicholls, J., 1967, Iron-titanium oxides and oxygen fugacities in volcanic rocks: Jour. Geophys. Research, v. 72, p. 4665-4687.

Chayes, Felix, 1966, Alkaline and subalkaline basalts: Am. Jour. Sci., v. 264, p. 128-145.

Darken, L. S., and Gurry, R. W., 1946, The system iron-oxygen II. Equilibrium and thermodynamics of liquid oxide and other phases: Am. Chem. Soc. Jour., v. 68, 798-816.

Engel, A. E. J., Engel, C. G., and Havens, R. G., 1965, Chemical characteristics of oceanic basalts and the upper mantle: Geol. Soc. America Bull., v. 76, p. 719-734.

Fudali, R. F., 1965, Oxygen fugacities of basaltic and andesitic magmas: Geochim. et Cosmochim. Acta, v. 29, p. 1063-1075.

Gass, I. G., 1967, Geochronology of the Tristan da Cunha Group of Islands: Geol. Mag., v. 104, p. 160-170.

Häkli, T. A., and Wright, T. L., 1967, The fractionation of nickel between olivine and augite as a geothermometer: Geochim. et Cosmochim. Acta, v. 31, p. 877-884.

Kennedy, G. C., 1948, Equilibrium between volatiles and iron oxides in igneous rocks: Am. Jour Sci., v. 246, p. 529-549.

Larson, H., and Chipman, J., 1953, Oxygen activity in iron oxide slags: Am. Inst. Mining Metall. Petroleum Engineers Trans., v. 197, p. 1089-1096.

Le Maitre, R. W., 1962, Petrology of volcanic rocks, Gough island, south Atlantic: Geol. Soc. America Bull., v. 73, p. 1309-1340.

Muan, Arnulf, and Osborn, E. F., 1956, Phase equilibria at liquidus temperatures in the system MgO-FeO-Fe_2O_3-SiO_2: Am. Ceramic Soc. Jour., v. 39, p. 121-140.

Paul, A., and Douglas, R. W., 1965, Ferrous-ferric equilibrium in binary alkali silicate glasses: Physics and Chemistry of Glasses, v. 6, p. 207-211.

Peck, D. L., Wright, T. L., and Moore, J. G., 1966, Crystallization of tholeiitic basalt, Alae lava lake, Hawaii: Bull. Volcanol., v. 29, p. 629-656.

Sato, M., and Wright, T. L., 1966, Oxygen fugacities directly measured in magmatic gases: Science, v. 153, p. 1103-1105.

Shibata, Kenji, 1967, The oxygen partial pressure of the magma from Mihara volcano, O-Sima, Japan: Chem. Soc. Japan, Bull., v. 40, p. 830-834.

Smith, J. V., 1965, X-ray emission microanalysis of rock-forming minerals I. Experimental techniques: Jour. Geology, v. 73, p. 830-864.

Speidel, D. H., 1967, Effect of MgO on hematite-ilmenite magnetite-ulvospinel equilibria [abs.]: Am. Geophys. Union Trans., v. 48, p. 225.

Taylor, R. W., 1964, Phase equilibria in the system FeO-Fe_2O_3-TiO_2 at 1300°C: Am. Mineralogist, v. 49, p. 1016-1030.

Watkins, N. D., and Haggerty, S. E., 1967, Primary oxidation variation and petrogenesis in a single lava: Beitr. Mineralogie Petrologie, v. 15, p. 249-269.

Webster, A. H., and Bright, N. F. H., 1961, The system iron-titanium-oxygen at 1200°C and oxygen partial pressures between 1 atm and 2×10^{-14} atm: Am. Ceramic Soc. Jour., v. 44, p. 110-116.

Wright, T. L., and Weiblen, P. W., 1967, Mineral composition and paragenesis in tholeiitic basalt from Makaopuhi lava lake, Hawaii [abs.]: Geol. Soc. America, Ann. Mtg., New Orleans, 1967, Program, p. 242-243.

Yoder, H. S., Jr., and Tilley, C. E., 1962, Origin of basalt magmas: an experimental study of natural and synthetic rock systems: Jour. Petrology, v. 3, p. 342-532.